LITHOS 456-457 (2023) 107328

Contents lists available at ScienceDirect

LITHOS

journal homepage: www.elsevier.com/locate/lithos

# Disequilibrium in historic volcanic rocks from Fogo, Cape Verde traces carbonatite metasomatism of recycled ocean crust

A.K. Barker [a,b,*], E. Magnusson [a], V.R. Troll [a,b,c], C. Harris [d], H.B. Mattsson [e,a], P.M. Holm [f], F.J. Perez-Torrado [c], J.C. Carracedo [c], F.M. Deegan [a,b]

[a] Department of Earth Sciences, Uppsala University, Uppsala, Sweden
[b] Centre of Natural Hazards and Disaster Sciences (CNDS), Uppsala, Sweden
[c] Instituto de Estudios Ambientales y Recursos Naturales (iUNAT), Universidad de Las Palmas de Gran Canaria (ULPGC), Las Palmas de Gran Canaria 35017, Spain
[d] Department Geological Sciences, University of Cape Town, Cape Town, South Africa
[e] Institute for Mineralogy and Petrology, ETH Zürich, Switzerland
[f] Department of Geosciences and Natural Resource Management, University of Copenhagen, Øster Voldgade 10, Copenhagen 1350, Denmark

ARTICLE INFO

*Keywords:*
Fogo, Cape Verde
Volcanic rocks
Magma hybridization
Mantle heterogeneity
Oxygen isotopes
Carbonated eclogite

ABSTRACT

Fogo, Cape Verde, located upon thick oceanic lithosphere, provides a window into processes occurring in the mantle where recycled ocean crust in an upwelling mantle plume interacts with ambient mantle. Our objective is to investigate the nature of the lithologies of the mantle sources involved in the petrogenesis of historic volcanic rocks from Fogo. We observe enclaves and mingling textures in the lavas combined with oxygen isotope disequilibrium between olivine and clinopyroxene phenocrysts. Olivine $\delta^{18}O$ values display positive correlations with Zr/Hf and Zr/Y and a negative correlation with U/Th, whereas clinopyroxene $\delta\ ^{18}O$ values correlate positively with Ba/Nb. Heterogeneity between crystal populations and within the groundmass indicates that multiple magma batches are mixed beneath Fogo. In terms of mantle endmembers and source lithologies, a HIMU endmember was generated by melting of carbonated eclogite as indicated by low $\delta\ ^{18}O$ values, Zr/Hf, Ba/Nb and high U/Th ratios. In contrast, we show the EM1 endmember has high $\delta\ ^{18}O$, Zr/Hf, Ba/Nb and low U/Th ratios, derived from melting of variably carbonated peridotite. Additionally, Ba/Th ratio are high, indicating that carbonatite melts have contributed to alkaline magma compositions at Fogo.

## 1. Introduction

Ocean Island magmas generally experience limited assimilation as they pass through the ocean crust and, consequently, they allow the composition of the mantle source to be constrained (e.g. Gast, 1968; O'Hara, 1965; O'Nions et al., 1976). This is the underlying premise for exploring mantle source heterogeneity at Ocean Islands and has been widely used globally to assess mantle heterogeneity (e.g. Barker et al., 2010; Dalrymple et al., 1973; Escrig et al., 2005; Gerlach et al., 1988; Hofmann et al., 1986; Holm et al., 2006).

The Cape Verde Archipelago displays distinct geochemical heterogeneity whereby the northern islands show affinity to HIMU-like (High $\mu = {}^{238}U/{}^{206}Pb$) and local Depleted MORB Mantle (DMM) components (Davies et al., 1989; Doucelance et al., 2003; Gerlach et al., 1988; Holm et al., 2006; Millet et al., 2008). In contrast, the southern islands of Fogo, Santiago and Maio are supplied by HIMU-like and enriched mantle (EM1) components (Barker et al., 2009, 2010; Davies et al., 1989; Doucelance et al., 2003; Escrig et al., 2005; Gerlach et al., 1988; Hildner et al., 2011; Martins et al., 2009; Mata et al., 2017). Notably, the Cadamosto seamount at the southwestern tip of the southern island chain is geochemically more similar to the northern island chain with a mixed HIMU-like and local DMM mantle source (Barker et al., 2012). On the neighbouring island of Brava, there is a temporal distinction with similar characteristics to the northern islands until 0.5 Ma, when the EM1-like component appears (Mourão et al., 2012). Carbonatites are present in the Cape Verde Archipelago, including on the island of Fogo and recent studies have shown high volatile contents and associated deep exsolution of $CO_2$ beneath Fogo (DeVitre et al., 2023; Hoernle et al., 2002).

Furthermore, several studies have investigated geochemical indicators of mantle source lithology at Cape Verde. The lavas have been shown to be globally amongst the Ocean Islands that display high $TiO_2$

* Corresponding author at: Department of Earth Sciences, Uppsala University, Uppsala, Sweden.
*E-mail address:* abigail.barker@geo.uu.se (A.K. Barker).

https://doi.org/10.1016/j.lithos.2023.107328
Received 6 April 2023; Received in revised form 11 August 2023; Accepted 11 August 2023
Available online 15 August 2023

contents of 3 to 5 wt%, which has been proposed to be associated with a pyroxenitic source (Prytulak and Elliott, 2007). Barker et al. (2010) investigated the major element compositions of lavas from Santiago and showed that they are consistent with involvement of pyroxenite and carbonated eclogite source lithologies. Olivine Ni and Mn compositions from Santiago and Santo Antão are consistent with a complex mixed eclogite-pyroxenite-peridotite source contributing to melt compositions (Barker et al., 2014).

Partial melting of peridotite produces ultramafic melts, with low $TiO_2$ contents <1.5 wt% (Hirose and Kushiro, 1993). Ocean crust that has been subducted and transformed into eclogite is thought to be recycled at Ocean Islands in the form of HIMU-like mantle heterogeneities. Pure eclogitic melts of recycled ocean crust are expected to have andesitic compositions (Sobolev et al., 2000; Spandler et al., 2008). These andesitic melts react with peridotite to form pyroxenite, in turn when the pyroxenite melts the corresponding ultramafic melts have higher $TiO_2$ contents (1.1 to 3.4 wt% $TiO_2$, Hirschmann et al., 2003, Kogiso et al., 2004; Sobolev et al., 2005). However, if eclogite is carbonated the resulting melts are Ti-rich ultramafic compositions with 33 to 43 wt% $SiO_2$ and 2.6 to 8.6 wt% $TiO_2$ (Dasgupta et al., 2006). Corresponding carbonated peridotite melts are also ultramafic with $TiO_2$ compositions of 0.5 to 1.9 wt% (Dasgupta et al., 2007).

We present whole rock major and trace element data combined with oxygen isotope compositions of mineral and groundmass separates for samples of volcanic rocks erupted inside the Chã das Caldeiras, Fogo. Our sample suite is composed of 58 whole rocks spanning historic eruptions from 1664 to 2014/2015 and a pre-historic lava. Olivine, clinopyroxene and groundmass separates were prepared for fourteen samples and analyzed for oxygen isotopes (Fig. 1; Tables S1 and S2). We employ these samples to constrain the lithologies associated with the mantle source heterogeneity.

### 1.1. Volcanism on Fogo

The Cape Verde archipelago is morphologically composed of three groups; the older highly eroded eastern islands, the northern islands and the southern islands (Fig. 1; Ramalho et al., 2010). Fogo island is located in the southern island chain and is the most volcanically active of the islands. It also hosted the most recent eruption at Cape Verde that occurred from November 2014 to February 2015 (Fernandez and Faria, 2015; González et al., 2015; Jenkins et al., 2017; Richter et al., 2016).

The evolution of the Island of Fogo can be divided into four main phases according to Day et al. (1999) and Foeken et al. (2009). The first phase involves the uplifted seamount series composed of carbonatite and alkaline basalts dated to ca. 4.5 Ma. The second phase, the Monte Barro Group, is comprised of the first subaerial lavas, which unconformably overlie the seamount series (Day et al., 1999; Foeken et al., 2009). The third phase features the stratovolcano Monte Amarelo that formed from a period of intense volcanism. The deposits of Monte Amarelo reached a total thickness of up to 3 km, and unconformably overlie the Monte Barro Group (Day et al., 1999; Foeken et al., 2009). The Monte Amarelo phase is probably of Quaternary age and ended with a lateral collapse of the volcano's summit at 68 ka (Cornu et al., 2021). The fourth phase of island evolution is composed of the Chã das Caldeiras Group volcanism that commenced c. 62 ka and continues to the present day (Foeken et al., 2009). During this time an approximately 2 km thick caldera infill built up in the collapse scar, forming the Chã das Caldeiras plain (Day et al., 1999; Foeken et al., 2009). This fourth phase also includes the conspicuous Pico de Fogo stratovolcano as well as discontinuous lava sequences of basanitic to tephritic composition on the outer flanks of the island (Day et al., 1999; Foeken et al., 2009).

Pico de Fogo volcano consists of layers of mafic pyroclastic deposits and lava that formed from persistent volcanic activity, from at least 1500 to 1785 CE (Worsley, 2015). Subsequent eruptions have emanated from the lower flanks of Pico de Fogo (Carracedo et al., 2015), including the latest eruption in 2014 to 2015 (Jenkins et al., 2017; Richter et al., 2016; Worsley, 2015). The historic eruptions are typically of Hawaiian and Strombolian style and are characterized by ash, bombs, scoria and lava flows. Historically, the eruptions usually have durations of approximately two months with an average recurrence frequency of around twenty years (Worsley, 2015). Recent eruptions have been chemically zoned with initial eruption of phonotephrites and later tephrites (Hildner et al., 2011, 2012; Klügel et al., 2020; Mata et al., 2017).

## 2. Methods

The analysis of whole rock major and trace elements was performed at ACME Analytical Laboratories Ltd. in Vancouver, Canada on twelve samples. Before the analysis, the samples were prepared by jaw crushing and milling. For major element analyses, 0.5 g of powdered material was first digested with a $LiBO_2/Li_2B_4O_7$ flux and then analyzed by inductively coupled plasma emission spectrometry (ICP-ES). For the trace element analyses, 0.25 g of sample powder was digested with an $HNO_3$-$HClO_4$-HF solution prior to analysis with inductively coupled plasma mass spectrometry (ICP-MS).

Additionally, 45 samples were prepared and analyzed at the Institute for Mineralogy and Petrology, ETH Zürich. They were crushed with a hydraulic ram containing a stainless-steel cast and powdered in an agate disc mill. Glass beads were produced by fusing sample powders mixed with lithium tetraborate at 950 °C for two hours. Major elements were analyzed by XRF using a Panalytical Axios wavelength-dispersive instrument. The glass beads were also used for trace element analysis by laser ablation inductively coupled plasma mass spectrometry (LA-ICP-MS), using a 193 nm wavelength ArF excimer laser connected to an Elan 6100 DRC ICP-MS. Laser apertures of 40 μm and 60 to 90 μm were used for ablating reference materials and samples, respectively. The NIST standard 610 was used for calibration following Taylor et al. (1997). Each sample was analyzed in triplicate and the raw data was processed using the SILLS software (Guillong et al., 2008).

The analytical precision for major elements was assessed using internal standards and a duplicate of one sample. Based on the duplicate, the analytical precision for elements with a concentration of <2.5 wt% gave a relative reproducibility of ≤1.1%, whereas for major elements with >2.5 wt% the relative reproducibility was ≤0.52%. The analytical precision for trace elements was estimated by comparison between the analytical standard determined at ACME and the deviation from the certified values. For most elements the deviation was from ca. 2 to 10% but some showed higher deviations and in general the deviation was greater at lower concentrations. The detection limit for oxides was 0.01%, whereas for trace elements it varied between 0.002 ppm and 1 ppm. The resulting data for whole rock major and trace elements are presented in Table S1 in the supplementary material. The compiled dataset shows clear liquid lines of descent that suggest the analytical uncertainties and interlaboratory bias is negligible.

The oxygen isotope composition of clinopyroxene, olivine and groundmass was measured for fourteen samples. The crystals chosen for the analysis had a mass of 2 to 3 mg each and they were hand-picked from sample material that had been previously crushed to sand-sized fragments in a jaw crusher. Groundmass chips were carefully selected to represent pristine material, free from visible crystals, before they were milled in an agate mortar. The oxygen isotope analysis was performed at the University of Cape Town in South Africa. For the olivine and clinopyroxene crystals, $\delta^{18}O$ values were determined using laser fluorination where the oxygen is released by heating with an infrared laser (9.6 μm $CO_2$) in the presence of 15 kPa $BrF_5$ (Harris and Vogeli, 2010). The oxygen was captured on 5 Å molecular sieve inside a glass bottle after being released from reaction of the samples. The $\delta^{18}O$ values for the groundmass were determined using a conventional silicate line according to methods described in Harris and Vogeli (2010). Groundmass chips were milled and approximately 10 mg of sample powder was reacted with 10 kPa of $ClF_3$ at 550 °C. The oxygen gas produced was

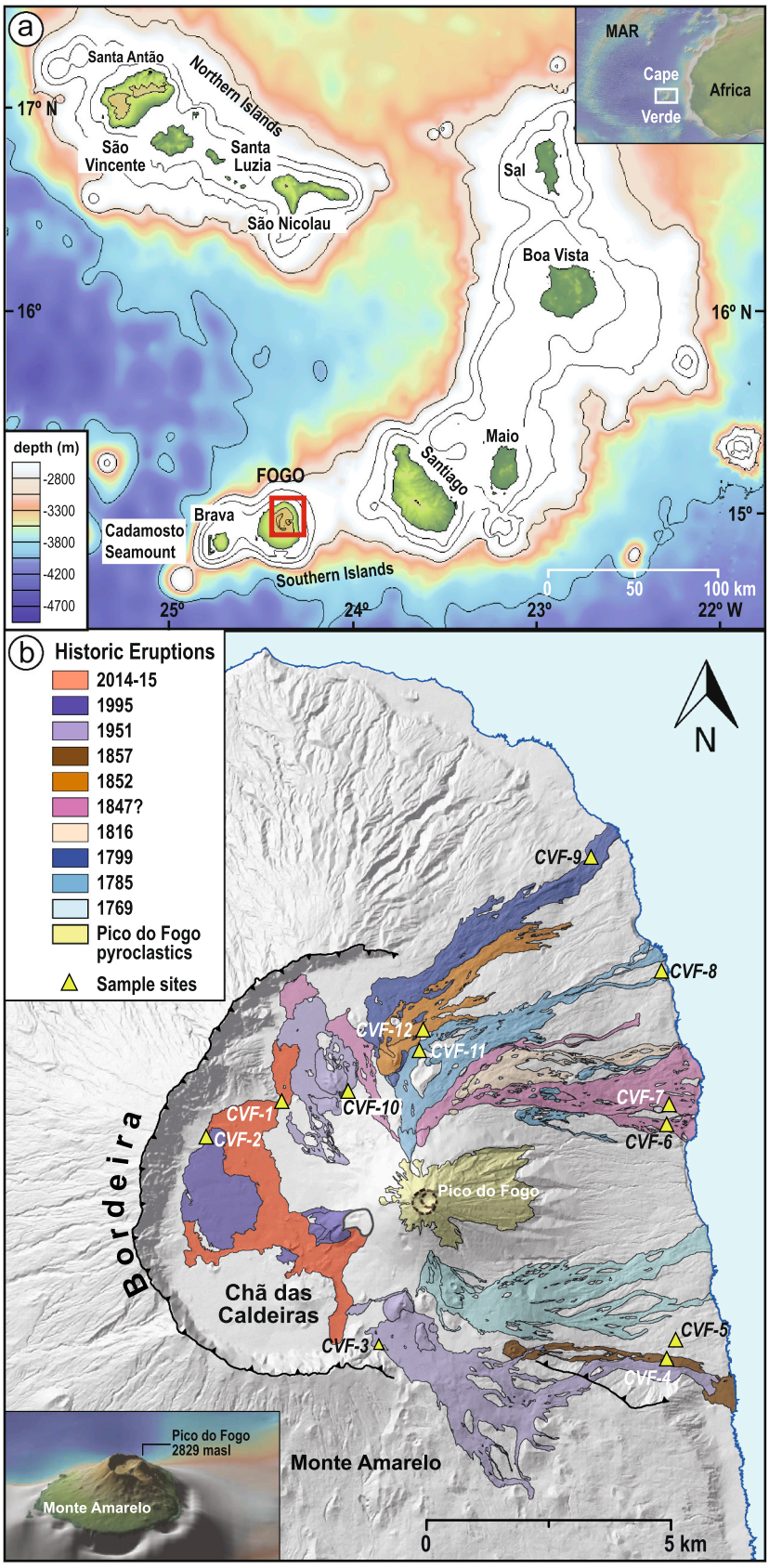


**Fig. 1.** A) The Cape Verde archipelago features Fogo, marked by the red square, in the southern island chain. The archipelago is located in the Central Atlantic as shown in the inset. B) Topography of Fogo Island. Monte Amarelo defines the form of Fogo Island (see inset). Pico de Fogo is located in the collapse scar in the Northeast of Fogo and historic eruption vents are located on the Chã das Caldeiras. Historic eruption deposits are shown following Carracedo et al. (2015). Maps are created in www.geomapapp.org (Ryan et al., 2009). (For interpretation of the references to colour in this figure legend, the reader is referred to the web version of this article.)

then converted to $CO_2$ by a hot platinized carbon rod. All isotope ratios were measured using a Thermo DeltaXP mass spectrometer. For groundmass separates, the quartz standard MQ was used as an internal reference standard, for which the long-term analytical precision is 0.16‰ (2σ; Harris et al., 2015). For the laser fluorination analysis of the minerals, MON GT was used as an internal standard and run in duplicate with each batch of 10 samples and was used to normalise the raw data to the SMOW scale. The long-term analytical precision is 0.15‰ (2σ) based on 216 duplicate analyses of MON GT. The $\delta^{18}O$ values are reported in Table S2 of the supplementary material.

## 3. Results

### 3.1. Petrography

Our samples display porphyritic textures with larger crystals of clinopyroxene and olivine dispersed in a microcrystalline to glassy groundmass (Fig. 2; $n = 12$ thin sections). The samples typically have approximately 20% phenocrysts although an ankaramite has 35% crystals (visually estimated by area), with crystal sizes ranging up to ca. 5 mm. Euhedral to subhedral clinopyroxene is the dominant crystal phase in all samples, usually constituting between 15 and 30% of the sample, followed by anhedral to subhedral olivine that constitutes ca. 1 to 8% of most samples. Opaque phases are present in all samples constituting up to 5%. Clinopyroxene and olivine often host apatite inclusions. A few corroded amphibole crystals were observed in samples from the eruptions in 1852, 1857 and 1951 (Fig. 2b). Hourglass, concentric and oscillatory zonation are common features in clinopyroxene crystals, whereas zonation is typically absent from olivine crystals (Fig. 2 a and d). Simple twinning in clinopyroxene is also common and some euhedral clinopyroxene crystals feature rounded cores. The groundmass is glassy to microcrystalline and mainly consists of clinopyroxene, olivine and opaques phases. In a few of these samples, plagioclase was found in the groundmass and nepheline was also observed. Glass is preserved in about half of the samples, representing several different eruptions. The glass is often found adjacent to vesicles and either forms patches or mingling textures with the holocrystalline groundmass (Fig. 2g). Additionally, small enclaves are not uncommon and are distinguished by dark grey to brown color, with finer grained groundmass than the host rock (Fig. 2h). Most enclaves display sharp contacts with the groundmass, although some are gradational. The enclaves often contain a few subhedral to anhedral phenocrysts of clinopyroxene, olivine and iron oxides, with smaller microcrysts and needles of clinopyroxene, plagioclase and iron oxides in a very fine-grained groundmass. One sample from the 2014/2015 eruption contains enclaves with a glassy groundmass.

Similar mineralogy has also been described for samples from the 2014/2015, 1995 and 1951 eruptions with the appearance of apatite in more evolved samples (Hildner et al., 2011, 2012; Klügel et al., 2020; Mata et al., 2017). The occurrence of minor feldspathoids, such as nepheline, leucite and melilitite has also been reported by Mata et al. (2017) and Hildner et al. (2011, 2012).

### 3.2. Major elements

The Fogo samples from this study are alkaline with $SiO_2$ of 40 to 50 wt% and total alkalis of 3.0 to 11.7 wt%, therefore they classify as tephrite-basanite to (mela)nephelinite and phonotephrite (Fig. 3a; Le Bas et al., 1985). In comparison to our sample set, data reported from other studies show a similar range of compositions (Fig. 3a; Davies et al., 1989; Doucelance et al., 2003; Escrig et al., 2005; Gerlach et al., 1988; Hildner et al., 2011, 2012; Mata et al., 2017). Additionally, patches of glass within samples from the 2014/2015 eruption range from tephrite to phonolite at 44 to 54 wt% $SiO_2$ with total alkalis of 8.4 to 15.6 wt% (Fig. 3a; Klügel et al., 2020; Mata et al., 2017). These patches of phonolitic glass are similar to silica-rich glass found in mantle xenoliths from Sal, which are phonolite to trachyte in composition (Fig. 3a; Bonadiman et al., 2005). Compared to samples from Fogo, eclogite melts have intermediate compositions with $SiO_2$ of 51 to 57 wt% at low total alkali contents of 1.9 to 4.7 wt% (Fig. 3a). Experimental peridotite melts are basaltic, whereas pyroxenite melts are basalt to tephrite-basanite in composition (Fig. 3a; 0.5 to 5 GPa; Hirose and Kushiro, 1993; Hirschmann et al., 2003; Kogiso et al., 2004). In addition, carbonated lithologies generate picrobasalt to basalt or picrobasalt to nephelinite for carbonated peridotite and carbonated eclogite respectively (Fig. 3a; Dasgupta et al., 2006, 2007).

The Fogo volcanic rocks have MgO contents of 1.8 to 11.8 wt% with $TiO_2$ contents that range from 1.9 to 4.1 wt% and below 8.5 wt% MgO the $TiO_2$ and MgO contents decrease simultaneously (Fig. 3b; Doucelance et al., 2003; Escrig et al., 2005; Eisele et al., 2016; Hildner et al., 2012; Mata et al., 2017). The glass from the 2014/2015 eruption extends down to 0.65 wt% MgO and 0.7 wt% $TiO_2$, overlapping with Sal mantle xenolith glass at 0.35 to 1.65 wt% MgO and 0.43 to 1.67 wt% $TiO_2$ with a few recording high $TiO_2$ of up to 3 wt% (Bonadiman et al., 2005; Klügel et al., 2020; Mata et al., 2017). The Fogo volcanic rocks display CaO contents of 6.3 to 14.0 wt%, and below 8.5 wt% MgO the trend with MgO is positive tracing a liquid line of descent (Fig. 3c; Doucelance et al., 2003; Escrig et al., 2005; Eisele et al., 2016; Hildner et al., 2012; Mata et al., 2017). Glass from the 2014/2015 eruption continues the trend to 0.99 wt% CaO, and the mantle xenolith glass has similarly low values down to 0.16 wt% CaO (Bonadiman et al., 2005; Klügel et al., 2020; Mata et al., 2017). The Fogo volcanic rocks show $K_2O$ compositions of 1.3 to 4.7 wt%, increasing as the MgO decreases (Fig. 3d; Doucelance et al., 2003; Escrig et al., 2005; Eisele et al., 2016; Hildner et al., 2012; Mata et al., 2017). Volcanic glass from the 2014/2015 eruption extends the trend up to 7.6 wt% $K_2O$ and overlaps with the mantle xenolith glass at 6.6 to 8.8 wt% $K_2O$ (Bonadiman et al., 2005; Klügel et al., 2020; Mata et al., 2017).

Experimental melts of different mantle lithologies compare best to the mafic high MgO volcanic rocks from Fogo. Peridotite and carbonated peridotite melts display the highest MgO contents, with higher CaO and $TiO_2$ in carbonated peridotite melts relative to peridotite melts (Fig. 3; Dasgupta et al., 2007; Hirose and Kushiro, 1993). Pyroxenite melts have lower $TiO_2$ than the Fogo volcanic rocks, whereas carbonated eclogite melts traverse the range of $TiO_2$ contents observed in the Fogo volcanic rocks (Fig. 3; Hirschmann et al., 2003; Kogiso et al., 2004; Dasgupta et al., 2006). Pyroxenite and carbonated eclogite melts both have similar CaO contents to the Fogo volcanic rocks (Fig. 3; Hirschmann et al., 2003; Kogiso et al., 2004; Dasgupta et al., 2006). Eclogite melts seem to form two groups, the first comes from melt inclusions with eclogitic characteristics that have high MgO, at similar CaO and $TiO_2$ compositions to peridotite melts (Fig. 3; Sobolev et al., 2000). The second group of eclogite melts include both experimental melts and melt inclusions, which show 1.97 to 6.3 wt% MgO and have either high or low $TiO_2$ contents at intermediate to high CaO and very low $K_2O$ content (Fig. 3; Pertermann et al., 2004; Sobolev et al., 2000).

### 3.3. Trace elements

For comparison of parental magmas, we have corrected the incompatible trace elements for fractional crystallization along the liquid line of descent to a parental value of MgO 8.5 wt% (c.f. Klein and Langmuir, 1987). The value of 8.5 wt% MgO was chosen, because above this, the literature data shows highly scattered major element compositions, therefore samples with higher MgO values were omitted (Fig. 3). Below 4 wt% MgO the majority of the compositions deviate from the liquid line of descent as the magma composition changes and therefore these values are not corrected. The following descriptions and discussion refer to the corrected values for both the samples presented in this study and the literature data for Fogo.

Previous research has shown that radiogenic isotope compositions of volcanic rocks from Fogo island are associated with HIMU and EM1

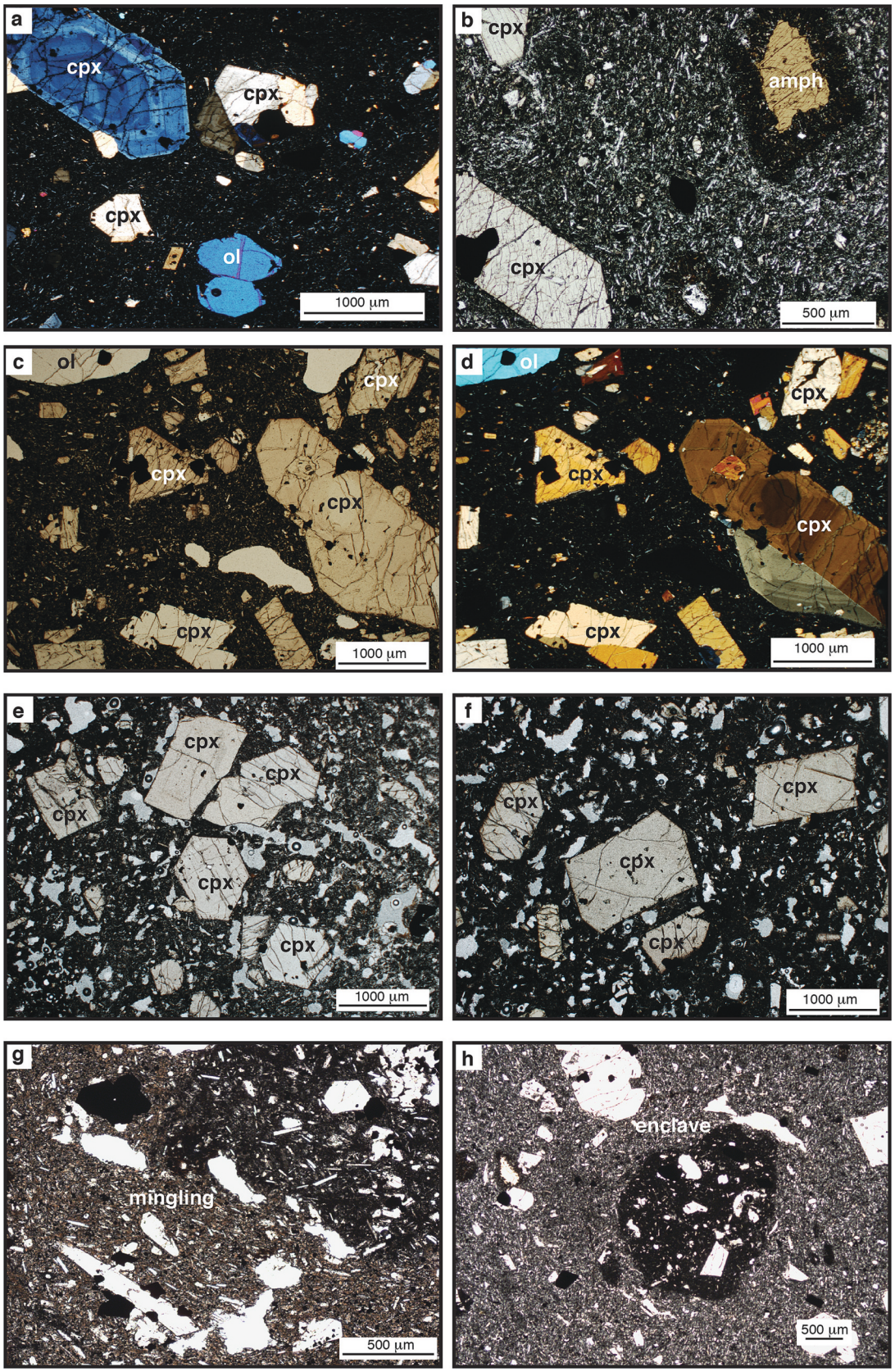


**Fig. 2.** Photomicrographs of representative samples from historic lavas of Fogo. The samples are clinopyroxene-olivine porphyritic with the occurrence of occasional amphibole xenocrysts. Cross polarized light highlights the frequent occurrence of zonation in clinopyroxene and the absence of zonation in olivine. Enclaves and mingling textures are present in the groundmass (g, h). (For interpretation of the references to colour in this figure legend, the reader is referred to the web version of this article.)

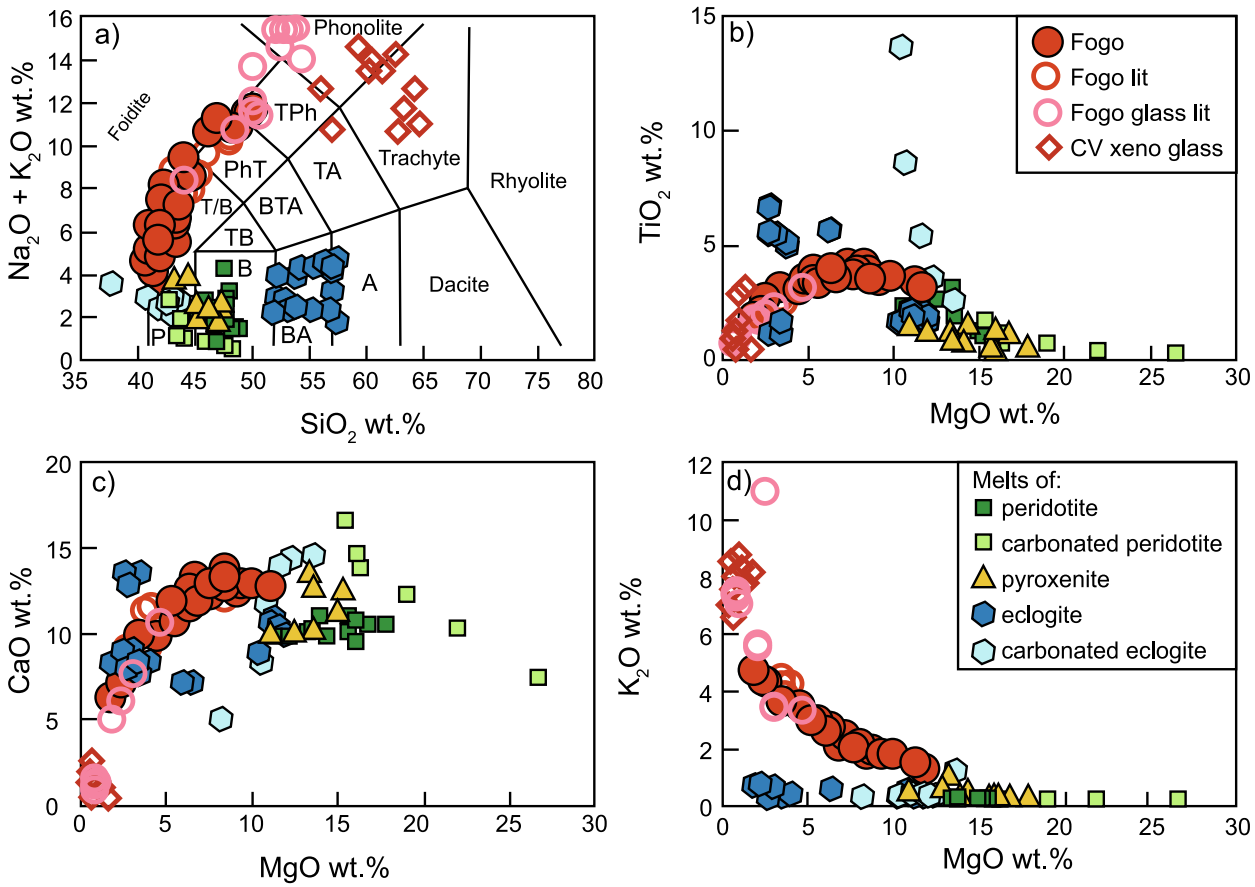


**Fig. 3.** Major element geochemistry for the Fogo volcanics from this study and the published data for Fogo. a) total alkali and silica diagram after Le Bas et al. (1985), b) $TiO_2$ vs MgO, c) CaO vs MgO, d) $K_2O$ vs MgO. Comparative data for Fogo come from Davies et al. (1989), Doucelance et al. (2003), Escrig et al. (2005), Gerlach et al. (1988), Hildner et al. (2011), Hildner et al., 2012), Klügel et al. (2020) and Mata et al. (2017). Experimental data and melt inclusions provide source lithologies for peridotite, carbonated peridotite, pyroxenite, eclogite and carbonated eclogite melts (Dasgupta et al., 2006, 2007; Hirschmann et al., 2003; Kogiso et al., 2004; Pertermann et al., 2004; Sobolev et al., 2000). (For interpretation of the references to colour in this figure legend, the reader is referred to the web version of this article.)

mantle components (Davies et al., 1989; Doucelance et al., 2003; Escrig et al., 2005; Gerlach et al., 1988). Hence we focus comparisons of the trace element geochemistry on mantle components from Ocean Island groups that most closely represent the HIMU and EM1 compositions. For HIMU we have used St. Helena and for EM1 we refer to Pitcairn and Tristan da Cunha (see supplementary materials for references).

Individual eruptions on Fogo have produced volcanic rocks with large ranges in trace element compositions, which dominate over potential variations with time. Our Fogo volcanic rocks have La/Sm of 3.63 to 6.22 and Zr/Hf of 34 to 53, following the increase in La/Sm and Zr/Hf displayed by the literature data from Fogo (Fig. 4a; Doucelance et al., 2003; Escrig et al., 2005; Eisele et al., 2016; Hildner et al., 2012; Mata et al., 2017). The Fogo volcanic rocks are similar to HIMU compositions from St. Helena (see supplementary materials for references). EM1 compositions from Tristan da Cunha and Pitcairn are also similar to our samples (see supplementary materials for references). Carbonatites from Fogo have high La/Sm and Zr/Hf compositions appearing as an extension of the trend of volcanic rock compositions (7 to 90 and 60 to 190 respectively; Doucelance et al., 2010; Hoernle et al., 2002).

We observe that the Fogo volcanic rock compositions form a cluster in Ba/Nb of 7.7 to 11.2 with Zr/Y of 8.1 to 13.5 (Fig. 4b). The literature data for Fogo volcanic rocks have higher Zr/Y of 10.8 to 13.0 than most of our samples at similar Ba/Nb of 7.5 to 13.4 (Fig. 4b; Doucelance et al., 2003; Escrig et al., 2005; Eisele et al., 2016; Hildner et al., 2012; Mata et al., 2017). Lavas with HIMU affinity have lower Ba/Nb of 4.5 to 6.4 and Zr/Y of 7.3 to 10.1 (see supplementary materials for references); Lavas from Tristan da Cunha with EM1 affinity are similar to the Fogo volcanic rocks with Ba/Nb of 7.8 to 14.5 and Zr/Y of 8.3 to 11.7 (see supplementary materials for references). Lavas from Pitcairn with EM1 affinity overlap with the Fogo volcanic rocks as well as the HIMU compositions, in contrast carbonatites have low Zr/Y compared to the volcanic rocks (see supplementary materials for references).

Fogo volcanic rocks exhibit Ba/La of 11.4 to 15.7, with the literature data ranging from 10.0 to 16.5, at U/Th of 0.19 to 0.33 (Fig. 4c; Doucelance et al., 2003; Escrig et al., 2005; Eisele et al., 2016; Hildner et al., 2012; Mata et al., 2017). Lavas with HIMU affinity, those resembling EM1 from Pitcairn and carbonatites mostly have lower Ba/La $\leq$11, whereas lavas with EM1 affinity from Tristan da Cunha have Ba/La of 10.0 to 15.8 and U/Th of 0.12 to 0.34 and compare well with the Fogo volcanic rocks.

The Fogo volcanic rocks cluster at Zr/Nb of 3.0 to 4.8 and Sr/Nd of 14 to 21, and the literature data overlap with our cluster of samples extending to Zr/Nb of 5.2 (Fig. 4d; Doucelance et al., 2003; Escrig et al., 2005; Eisele et al., 2016; Hildner et al., 2012; Mata et al., 2017). Lavas with HIMU affinity also cluster similarly to our samples at Zr/Nb of 3.5 to 5.5 and Sr/Nd of 11 to 17 (see supplementary materials for references). Lavas with EM1 affinity from Tristan da Cunha are similar to the Fogo volcanic rocks extending subvertically to higher Sr/Nd (Zr/Nb of 3.9 to 5.3 and Sr/Nd 14.5 to 28.5; see supplementary materials for references). Whereas lavas with EM1 affinity from Pitcairn have higher Zr/Nb 4.7 to 7.1, trending subparallel to lavas with EM1 sources from Tristan da Cunha at a wider range of Sr/Nd from 4 to 27 (see supplementary materials for references). Carbonatites from Fogo show either low or high Zr/Nb and Sr/Nd (Hoernle et al., 2002; Doucelance et al.,

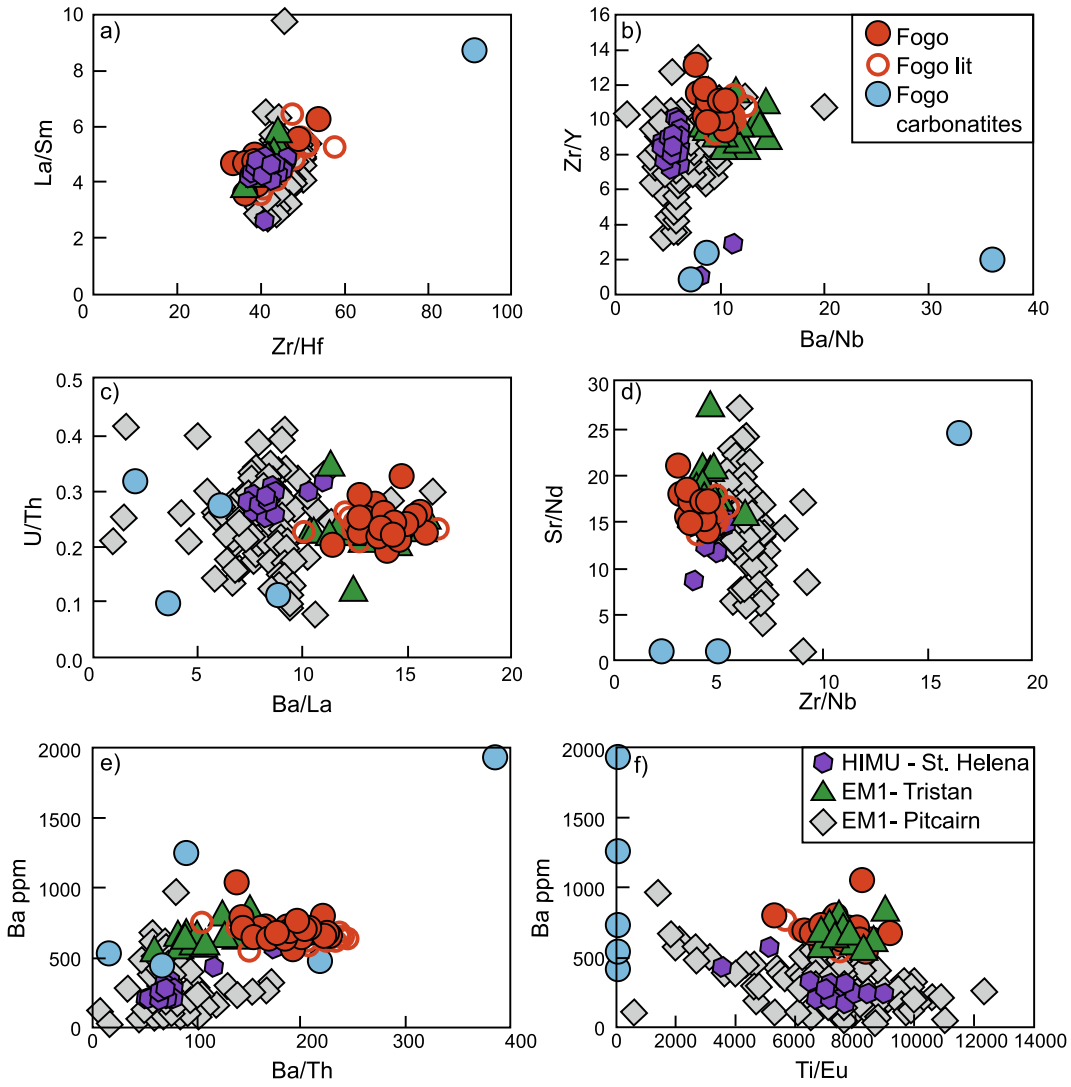


**Fig. 4.** Trace element ratios for the Fogo volcanic rocks, solid red circles depict the samples from this study, open red circles show the literature data (Davies et al., 1989; Doucelance et al., 2003; Escrig et al., 2005; Gerlach et al., 1988; Hildner et al., 2011, 2012; Mata et al., 2017). For the samples from this study as well as the literature data for Fogo, the trace elements have been corrected along the liquid line of descent to MgO 8.5 wt%, thus subtracting variations due to differentiation. For Fogo no significant correlations are found over time. The Fogo volcanic rocks are compared to carbonatites from Fogo (Doucelance et al., 2010; Hoernle et al., 2002), HIMU compositions from St. Helena, and EM1 compositions from Pitcairn and Tristan da Cunha (see supplementary materials for references). (For interpretation of the references to colour in this figure legend, the reader is referred to the web version of this article.)

2010).

Furthermore, Ba concentrations for the Fogo volcanic rocks are 545 to 1045 ppm and corresponding Ba/Th ratios range from 140 to 245 (Fig. 4e; this study; Doucelance et al., 2003; Escrig et al., 2005; Eisele et al., 2016; Hildner et al., 2012; Mata et al., 2017). Lavas with HIMU affinity show lower Ba and Ba/Th than the Fogo volcanics, lavas with EM1 affinity from Tristan da Cunha have similar Ba concentrations at lower Ba/Th ratios compared to the Fogo volcanics. Additionally, lavas with EM1 affinity from Pitcairn have lower Ba concentrations and lower Ba/Th ratios than the Fogo volcanics (see supplementary materials for references). Suitably high Ba concentrations and Ba/Th ratios are found in a few of the carbonatites from Fogo (Fig. 4e; Doucelance et al., 2010; Hoernle et al., 2002). The Fogo volcanic rocks have Ti/Eu of 5300 to 9200, which are very similar to EM1 from Tristan da Cunha and at lower Ba the Ti/Eu is comparable to lavas with HIMU affinity and EM1 from Pitcairn (Fig. 4f). The trends in Ba versus Ti/Eu for the Fogo and Pitcairn volcanic rocks are elongated towards carbonatite compositions at low Ti/Eu (see supplementary materials for references).

### 3.4. Oxygen isotopes

Olivine crystals in the volcanic rocks from Fogo have $\delta^{18}O$ values that range from 4.94 to 5.36‰, averaging 5.15‰, which is within error of the $\delta^{18}O$ value of depleted mantle olivine of 5.2 ± 0.2‰ (Fig. 5; Table S2; Eiler, 2001). For comparison, olivine from MORB show $\delta^{18}O$ values of 5.0 to 5.25‰ and HIMU olivine gives $\delta^{18}O$ values from 4.7 to 5.2‰ (Eiler, 2001). In comparison to ocean islands with EM1 compositions, olivine from Pitcairn displays $\delta^{18}O$ values of 5.1 to 5.3‰ and Tristan da Cunha and Gough Island have $\delta^{18}O$ values from 4.9 to 5.9‰ (Eiler et al., 1995, 1997; Harris et al., 2000).

Clinopyroxene from the Fogo volcanic rocks has $\delta^{18}O$ values that range from 4.81 to 5.37‰ with an average of 5.08‰, which is below the depleted mantle range for clinopyroxene (5.5‰ Bindeman et al., 2004; Fig. 5; Table S2). Clinopyroxene from the nearby Cadamosto Seamount show $\delta^{18}O$ of 5.3 to 5.4‰ which are within the depleted mantle range (Barker et al., 2012). Clinopyroxene from Tristan da Cunha and Gough Island, representing EM1 compositions, have $\delta^{18}O$ of 5.3 to 5.9‰ (Harris et al., 2000).

Fogo groundmass separates have $\delta^{18}O$ values that range from 5.36 to

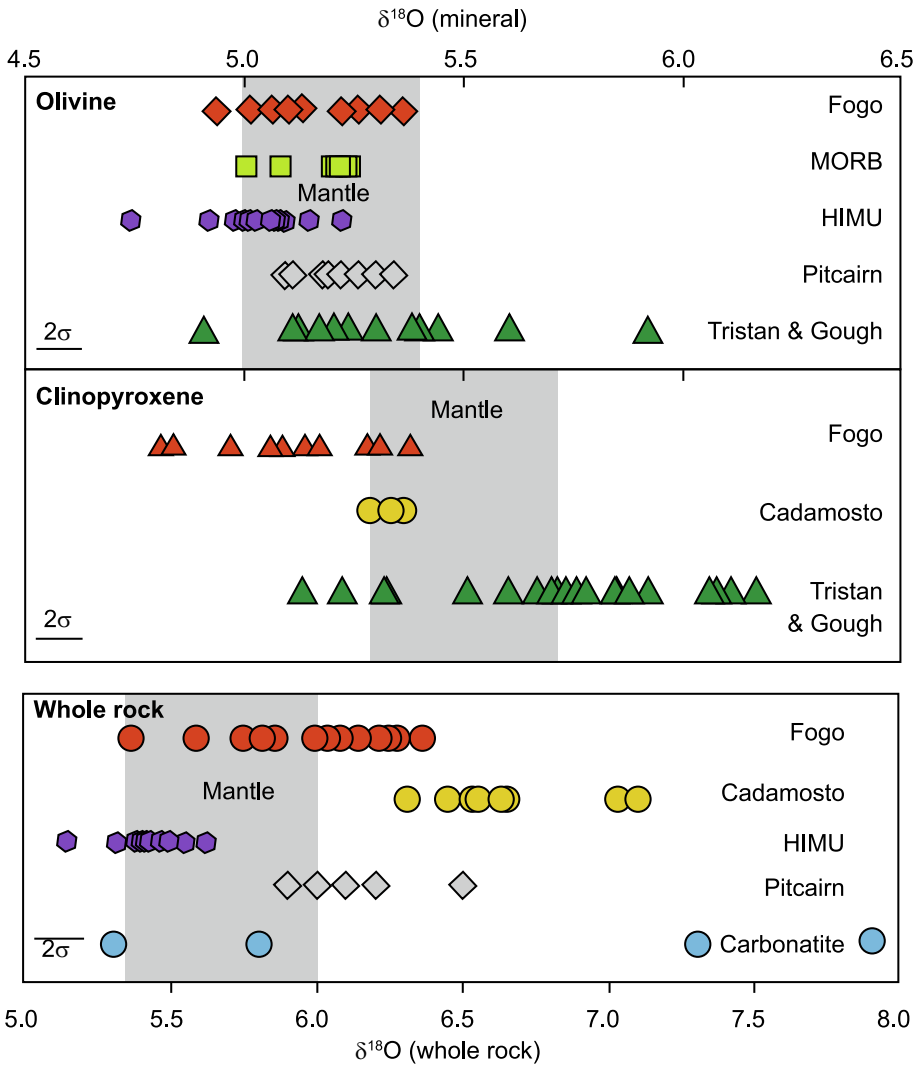


**Fig. 5.** Oxygen isotope data for olivine, clinopyroxene and groundmass from the historic volcanic rocks from Fogo. Comparison to MORB, HIMU, EM1 from Pitcairn, Tristan da Cunha and Gough Island, the Cadamosto Seamount and Carbonatites from Fogo (Barker et al., 2012; Eiler et al., 1995, 1997; Harris et al., 2000; Hoernle et al., 2002; Woodhead et al., 1993). Whole rock HIMU calculated as equilibrium melt from $\delta^{18}O$ olivine values with a Δol-gm of +0.4‰ (Eiler et al., 1997). Values for depleted mantle refer to Bindeman et al. (2004), Eiler (2001) and Ito et al. (1987). For Fogo no systematic correlations are found with oxygen isotopes over time. (For interpretation of the references to colour in this figure legend, the reader is referred to the web version of this article.)

6.36‰ and are similar to and higher than the normal range for depleted mantle (Table S2; Fig. 5; $\delta^{18}O$ 5.7 ± 0.3‰; Eiler, 2001; Ito et al., 1987). The loss on ignition (LOI) for our samples is 0.03% to 0.67% with an average of 0.48%. The $\delta^{18}O$ values do not show any correlation with LOI, alkali or large ion lithophile elements such as $K_2O$, Rb and Ba that would indicate alteration. Additionally, the freshest samples collected only months after the eruption in 2014/2015 have a wide range in groundmass $\delta^{18}O$ values of 5.36 to 6.14‰. Groundmass from phonolites to phonotephrites at the Cadamosto Seamount show $\delta^{18}O$ of 6.3 to 7.1‰. For comparison, the HIMU endmember from Madeira has $\delta^{18}O$ of 5.2‰ and globally lavas with HIMU affinity have $\delta^{18}O$ compositions of 5.1 to 5.6‰ (calculated melt in equilibrium with olivine; Δol-gm = +0.4‰; Eiler et al., 1997; Mata and Kerrich, 2000). Whereas $\delta^{18}O$ values of 5.9 to 6.5‰ are associated with EM1 compositions from Pitcairn (Fig. 5c; Woodhead et al., 1993). Additionally, primary carbonatites from Fogo have $\delta^{18}O$ 5.3 to 7.9‰ consistent with global occurrences of primary carbonatites with $\delta^{18}O$ values of 6 to 10‰ (Hoernle et al., 2002; Taylor Jr et al., 1967).

The difference in $\delta^{18}O$ value between clinopyroxene and olivine (Δcpx-ol) ranges from +0.02 to −0.34‰ with an average of −0.15‰ (±0.13 1 s.d.; Fig. 6a). At equilibrium, the expected difference between clinopyroxene and olivine $\delta^{18}O$ values (Δcpx-ol) is +0.49‰ at 1100 °C (Chiba et al., 1989). Therefore, the Fogo volcanic rocks appear to show oxygen isotope disequilibrium between olivine and clinopyroxene. Likewise, olivine displays offsets from groundmass of −0.1 to −1.3‰ (Δol-gm; mean − 0.79 ± 0.37‰ 1 s.d.; Fig. 6b). We see a similar relationship between clinopyroxene and groundmass with Δcpx-gm of −0.2 to −1.4‰ (mean − 0.94 ± 0.33‰ 1 s.d.; Fig. 6c). Compared to experimentally derived fractionation that corresponds to Δcpx-gm of −0.71 to −0.74‰ for basalt to tephrite, the Fogo volcanic rocks show a wide range (Zhao and Zheng, 2003). The range in Δcpx-gm obtained for the Fogo volcanic rocks is comparable to nephelinite at −0.16‰ and trachyandesite at −1.34‰ (Zhao and Zheng, 2003). The Δcpx-ol values are likely to be more reliable than Δcpx-gm and Δol-gm, because the two minerals were analyzed by the same method.

Oxygen isotope compositions of the Fogo volcanic rocks correlate with several whole rock trace element ratios. Olivine shows positive correlations between $\delta^{18}O$ and Zr/Hf as well as with Zr/Y and a negative correlation with U/Th ($r^2$ = 0.62, 0.55 and 0.57 respectively; Fig. 7). Meanwhile clinopyroxene displays positive correlations with whole rock Ba/Nb and Ba ($r^2$ = 0.68 and 0.50 respectively). Olivine $\delta^{18}O$ values do not correlate with Ba/Nb or Ba and likewise clinopyroxene $\delta^{18}O$ values do not show correlations with Zr/Hf, Zr/Y and U/Th. There are no such significant variations between whole rock geochemistry and groundmass oxygen isotope signatures.

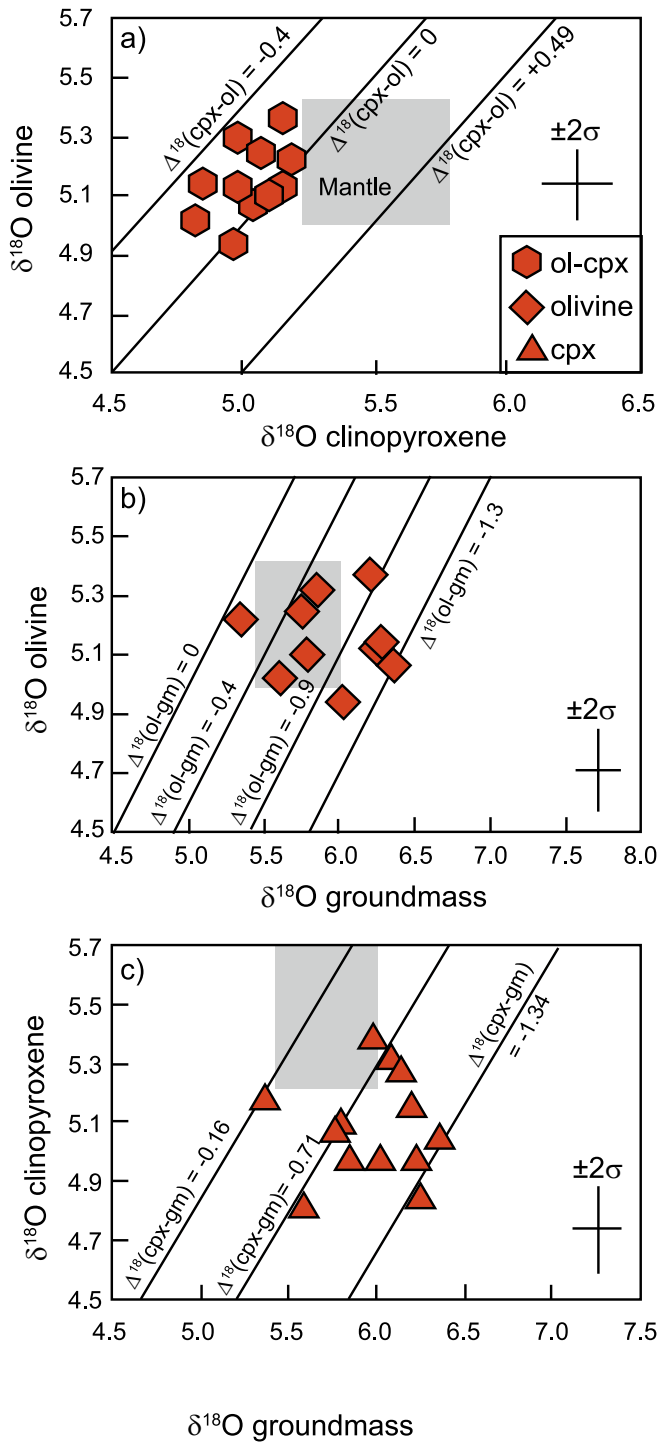


**Fig. 6.** Comparison of oxygen isotope data in different mineral phases and between minerals and groundmass for the Fogo volcanic rocks. a) olivine versus clinopyroxene, b) olivine versus groundmass and c) clinopyroxene versus groundmass. Black lines show the fractionation factors. Mantle values refer to Bindeman et al. (2004), Eiler (2001) and Ito et al. (1987). (For interpretation of the references to colour in this figure legend, the reader is referred to the web version of this article.)

## 4. Discussion

### 4.1. Disequilibrium

Volcanic rock samples are composed of phenocrysts, antecrysts and groundmass in different proportions and therefore the resulting whole rocks are compositional blends (e.g. Blundy and Shimizu, 1991; Davidson et al., 2007; Tepley III et al., 1999). The crystals found in lavas and tephra from individual eruptions may have grown from different magma compositions and under varying conditions and the groundmass may also reflect hybridisation of different magmas (Mollo et al., 2018). This type of within-magma heterogeneity is common in many systems (e.g. Barker et al., 2009; Bryce and DePaolo, 2004; Davidson et al., 2007). Here we examine the Fogo volcanic rock samples for evidence of disequilibrium and consider the construction of the final erupted assemblages.

The volcanic rocks from a variety of eruptions at Fogo display multiple features of heterogeneity. Some samples preserve enclaves with distinct mineral proportions such as more iron oxides compared to the groundmass (Fig. 2). Other samples have captured mingling textures between different magmas and others display fresh glass, often adjacent to vesicles indicating quenching during magma degassing. This textural heterogeneity is confirmed by the geochemistry, shown by the contrast in composition of glass compared to the host lava for the 2014/2015 eruption. Where the whole rock compositions are tephrite with minor phonotephrite and tephriphonolite, the glass compositions are mostly phonotephrite to phonolite (Fig. 3; Klügel et al., 2020; Mata et al., 2017). Furthermore, the glass compositions have A/CNK values of 0.87 to 1.49 which are mostly peraluminous with few metaluminous glass compositions analyzed ($n = 3/15$; Klügel et al., 2020; Mata et al., 2017). Such peraluminous compositions are unlikely to be derived by simple differentiation of a mafic magma, and thus support the presence of intra-sample heterogeneity.

Furthermore, oxygen isotope heterogeneity is also present. In the Fogo volcanic rocks $\Delta^{18}$Ocpx-ol ranges from unity to −0.34‰, compared to expected fractionation of Δcpx-ol +0.3 to +0.49‰ (Bindeman et al., 2004; Chiba et al., 1989; Eiler, 2001). We therefore conclude that there was oxygen isotope disequilibrium between the olivine and clinopyroxene in most of the samples. Furthermore, the $\delta^{18}$O values for the Fogo volcanic rocks indicate that olivine formed from a depleted mantle source with olivine $\delta^{18}$O values of 4.94 to 5.36‰ (average olivine from depleted mantle 5.2‰, Fig. 6a; Eiler, 2001). Whereas clinopyroxene is derived from a source with lower $\delta^{18}$O than depleted mantle with clinopyroxene $\delta^{18}$O values of 4.81 to 5.37‰ (average clinopyroxene from depleted mantle 5.5‰, Fig. 6a; Bindeman et al., 2004). Likewise, differences between olivine and groundmass ($\Delta^{18}$Ool-gm) display a large range of −0.1 to −1.3‰. Given the olivine $\delta^{18}$O values are consistent with crystallization from mantle derived magmas, we consider that the groundmass $\delta^{18}$O values are generally too high for equilibrium with the olivine crystals (Fig. 6b). Assuming oxygen isotope equilibrium between host magma and olivine during olivine crystallization, the $\delta^{18}$O values of the rocks are more variable than the olivine they contain. Similarly, we see a wider than expected difference between clinopyroxene and host groundmass $\delta^{18}$O values ($\Delta^{18}$Ocpx-gm -0.2 to −1.4‰; Fig. 6c). Both the clinopyroxene and groundmass appear to be out of equilibrium with depleted mantle compositions, with clinopyroxene tending towards lower $\delta^{18}$O values and groundmass showing elevated $\delta^{18}$O values (Fig. 6c). Taking into consideration the analytical uncertainties, an extremely wide crystallization interval would be required to produce the variation in clinopyroxene $\delta^{18}$O from a liquid with uniform $\delta^{18}$O under equilibrium conditions (Zhao and Zheng, 2003). Instead if we consider this range in $\Delta^{18}$Ocpx-gm at Fogo to be a primary magmatic feature, it is similar to the experimental range of clinopyroxene-melt fractionation with composition ranging from nephelinite to trachyandesite ($\Delta^{18}$Ocpx- melt -0.16 to −1.34‰; Zhao and Zheng, 2003). The corresponding clinopyroxene crystals have compositions mostly in the range 60 to 85 Mg#, however the data also feature groups of clinopyroxene at 45 to 60 Mg# and 10 to 20 Mg# (Barker et al., 2021). This wide range of clinopyroxene compositions is consistent with equilibrium growth within a wide range of magma compositions. The phonolite and phonotephrite glass present in tephrite samples from the 2014/2015 eruption confirms the apparent paradox of

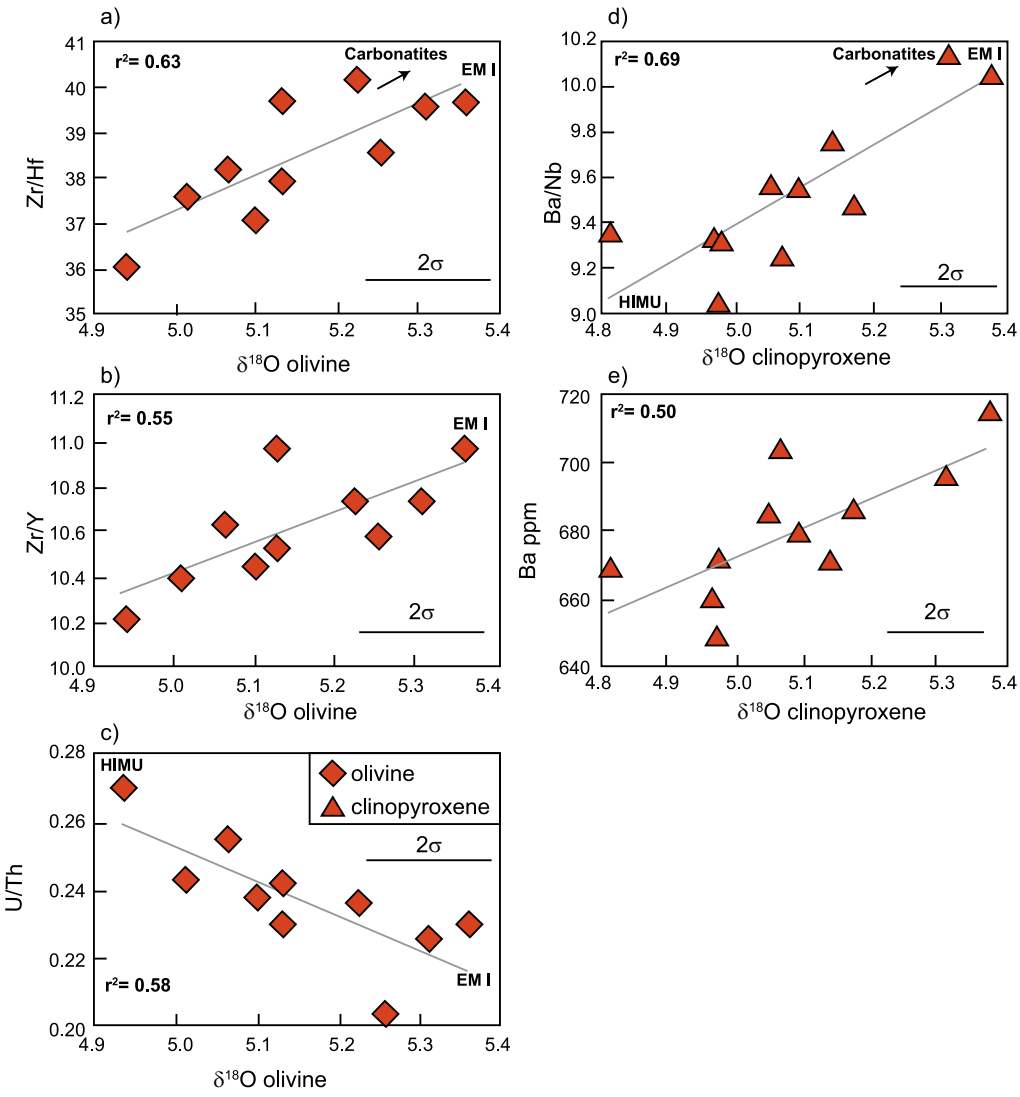


**Fig. 7.** Oxygen isotope composition for olivine and clinopyroxene plotted against whole rock trace element data. A) Zr/Hf vs. $\delta^{18}O$ olivine, b) Zr/Y vs. $\delta^{18}O$ olivine, c) U/Th vs. $\delta^{18}O$ olivine, d) Ba/Nb vs. $\delta^{18}O$ clinopyroxene and e) Ba concentration vs. $\delta^{18}O$ clinopyroxene. The corresponding correlation coefficients ($r^2$) for $\delta^{18}O$ clinopyroxene versus the following trace element ratios are Zr/Hf 0.016, Zr/Y 0.017 and U/Th 0.003. For $\delta^{18}O$ olivine we observe correlation coefficients of <0.0001 with Ba/Nb and 0.012 with Ba. The trace elements have been corrected along the liquid line of descent to MgO 8.5 wt%. (For interpretation of the references to colour in this figure legend, the reader is referred to the web version of this article.)

simultaneous clinopyroxene crystallization in equilibrium with mafic and felsic alkaline melts (Fig. 3; Klügel et al., 2020; Mata et al., 2017). Additionally, phonolitic to trachytic melts are involved in metasomatism of mantle xenoliths from Sal, consistent with felsic compositions being present within the mantle below Cape Verde, not just a feature of the magma plumbing system (Fig. 3; Bonadiman et al., 2005). Furthermore, different whole rock trace element ratios correlate with oxygen isotope values of olivine and clinopyroxene, indicating each phase and the whole rock composition represents mixing between different magma compositions (Fig. 7). We conclude, therefore, that there is disequilibrium between, and amongst, olivine, clinopyroxene and host magmas. This disequilibrium indicates that several populations of antecrysts and multiple magma compositions were involved in the genesis of these samples.

Disequilibrium and heterogeneity in the Fogo volcanic rocks were probably produced by mingling and hybridization of different proportions of mafic and felsic alkaline melts. Mixing between mafic and felsic melts is complementary to differentiation trends observed in the Fogo volcanic rock suite (Fig. 3). Therefore distinguishing the contribution of mixing from fractional crystallization is challenging. Additionally, we observe antecrysts that were formed in equilibrium with different magma compositions, which have been aggregated together in the final host magma. Thus the antecrysts record variations in magma compositions present deep in the magma storage system where olivine and clinopyroxene crystallize (Barker et al., 2021; Hildner et al., 2011, 2012; Klügel et al., 2020; Mata et al., 2017). It appears that a wide range of magma compositions was available during the entire evolution of the magmas erupted at Fogo. The temporal range of samples, for which we have petrographic and oxygen isotope data, span from 1799 to 2014/2015 plus a pre-historic sample (CV-05; Supplementary Table S1). Hence, they are consistent with diverse magma compositions being a long-lived feature of the deep magma storage zone (Barker et al., 2021; Carvalho et al., 2022; Hildner et al., 2011, 2012; Klügel et al., 2020; Leva et al., 2019; Mata et al., 2017). Additionally, we infer that felsic magmas play a long-term role in magma evolution even in the deep magma storage zone located in the lithospheric mantle. The roles of felsic melts and recharge of mafic magmas for mobilizing magma mush in connection with eruptions is uncertain. Although quenched phonolitic glass suggests that the final felsic melts have not been completely hybridized and some at least were injected not long before magma ascent and eruption.

### 4.2. Mantle source composition

The Cape Verde Archipelago displays distinct geochemical patterns, associated with archipelago scale heterogeneity (e.g. Barker et al., 2009, 2010, 2012; Davies et al., 1989; Doucelance et al., 2003; Gerlach et al., 1988; Holm et al., 2006; Mourão et al., 2012). These differences have

been ascribed to the involvement of various mantle source end members in the underlying mantle plume (e.g. Davies et al., 1989; Doucelance et al., 2003; Gerlach et al., 1988; Holm et al., 2006). The northern island chain is characterized by mixing of a local DMM and a HIMU-like component. In contrast, the southern island chain, including Fogo, shows contribution from an EM1-like component in addition to a HIMU-like component but no obvious DMM (Barker et al., 2009, 2010, 2012; Davies et al., 1989; Doucelance et al., 2003; Escrig et al., 2005; Gerlach et al., 1988; Holm et al., 2006).

The trace element data we present for the historic volcanic rocks on Fogo can mostly be explained by a combination of EM1 compositions, similar to Pitcairn and Tristan da Cunha, and HIMU compositions like Mt. St Helena (Fig. 4; see supplementary materials for references). The ratios of La/Sm, Zr/Nb, Sr/Nd and Zr/Y observed in the Fogo volcanic rocks can be produced by source components with either HIMU or EM1 compositions or both. Whereas Ba/La, U/Th and Ba/Nb require an EM1 component with possible influence from a HIMU component.

Correlations between trace element ratios and $\delta^{18}O$ value, where EM1 compositions of high Zr/Hf (40; $r^2 = 0.63$), low U/Th (0.22; $r^2 = 0.58$) and high Zr/Y (11; $r^2 = 0.55$), are associated with high $\delta^{18}O$ of 5.36‰ represent depleted mantle to EM1 compositions (Fig. 7). Additionally, the high $\delta^{18}O$ clinopyroxene endmember 5.37‰ has high Ba/Nb reflecting the involvement of an EM1 source component or a contribution of carbonatite (Fig. 7). Likewise, the low $\delta^{18}O$ olivine and clinopyroxene endmembers show trace element compositions e.g. U/Th ca. 0.28 and Ba/Nb ca. 9 respectively, that trend towards HIMU compositions (Fig. 7). This suggests that the low $\delta^{18}O$ endmember has incorporated more of the HIMU component, resulting in lower $\delta^{18}O$ values and associated trace element enrichment.

A few trace element compositions extend beyond EM1-HIMU compositions, such as the few samples which have high Zr/Hf or low Ti/Eu. This is clearest in Ba/Th, where most of the Fogo volcanic rocks have enriched Ba/Th ratios, extending away from the low ratios found in HIMU and EM1 (Fig. 4). Carbonatites from Fogo, display a range in Ba/Th from 16 to 1325 with an average of 430 ($n = 7$; Hoernle et al., 2002; Doucelance et al., 2003, 2010). Therefore, a contribution of carbonatite to the source of the magmas provides a likely explanation for the high Ba/Th ratios (Fig. 4). It is also noteworthy that the Fogo carbonatites display primary mantle $\delta^{18}O$ of 5.3 to 7.9‰ ($n = 4$, mean 6.6‰), overlapping with and extending to higher $\delta^{18}O$ than the Fogo volcanic rocks with $\delta^{18}O$ of 5.36 to 6.36‰ (groundmass; Fig. 5; Hoernle et al., 2002; Taylor Jr et al., 1967).

The groundmass $\delta^{18}O$ values span the depleted mantle range and extend to higher values (Fig. 5). However, they do not show any systematic variation with $SiO_2$ content, so fractional crystallization is unlikely to be the cause of the elevated $\delta^{18}O$ values. The phonolitic samples from the nearby Cadamosto Seamount show elevated $\delta^{18}O$ and $\delta^{34}S$, which was interpreted as minor assimilation of sediments (Barker et al., 2012). Hence any assimilation involved in the mafic Fogo magmas, which have lower $\delta^{18}O$ values than at the Cadamosto Seamount, would likely be negligible (Fig. 5). We ruled out effects of alteration above, therefore the high $\delta^{18}O$ values in the Fogo groundmass are likely to be inherited from the source and could either represent EM1 compositions or metasomatism of the source by carbonatite melts (Cornu et al., 2021).

In summary, the EM1 component present in the Fogo volcanic rocks leads to high $\delta^{18}O$ values in olivine, clinopyroxene and groundmass, together with high Zr/Hf, Zr/Y, Ba/Nb and low U/Th ratios. Likewise, the HIMU component is associated with low $\delta^{18}O$ for olivine and clinopyroxene associated with low Zr/Hf, Zr/Y, Ba/Nb and high U/Th ratios. Clinopyroxene displays the lowest $\delta^{18}O$ both in actual terms and relative to expected fractionation from mafic magma, suggesting that clinopyroxene crystals in equilibrium with phonolitic melt compositions are associated with the low $\delta^{18}O$ of the HIMU component.

### 4.3. Mantle source lithology

In order to assess the source lithologies involved in mantle melting to form the precursor magmas for the Fogo volcanic rocks, we have applied two strategies. Firstly, we compare the major element compositions with experimental melts and, secondly, we compare the trace element compositions with partial melting models of suitable mantle lithologies. The partial melting models are based on batch melting of peridotite, pyroxenite and eclogite (see supplementary information for details of modelling).

Major element compositions of experimental melts suggest that the primary magmas are potentially produced by carbonated peridotite to carbonated eclogite melts (Fig. 3). Interestingly, silica-rich partial melts of eclogite compare well to the CaO and $TiO_2$ compositions of phonotephrites from Fogo and glass compositions from the 2014/2015 eruption (Klügel et al., 2020; Mata et al., 2017). This suggests that eclogite melts may be playing a role alongside differentiation in generation of felsic compositions observed in the Fogo volcanic rocks. However, the experimental eclogite melts seem to have lower K content than the volcanic rocks and glasses observed from Fogo (Fig. 3d). This may be due to melting under different conditions in nature than the experimental eclogite melts. The presence of phonolitic to trachytic glass in mantle xenoliths from Sal, Cape Verde suggests that such felsic compositions were indeed present as melt at mantle depths. The combined evidence suggests these felsic melts were likely derived from melting of recycled lithologies in the mantle (Bonadiman et al., 2005).

Pyroxenite melts often have trace element compositions between eclogite melts, peridotite melts and their carbonated melts, reflecting formation by reaction of eclogite melts with peridotite (Fig. 8; Brown and Lesher, 2016; Sobolev et al., 2005). Partial melting models show that the Fogo volcanic rocks can explain the Zr/Hf, Zr/Y and Ba/Nb ratios by melting of carbonated eclogite melts and potentially a contribution of peridotite and eclogite melts (Fig. 8a, b). Whereas Ba/La ratios are between those of eclogite and peridotite melts (Fig. 8c). Additionally, Sr/Nd compositions for the Fogo volcanic rocks and pyroxenite melts are compositionally between eclogite melts, peridotite melts and their carbonated equivalents (Fig. 8d). The high Ba/Th and low U/Th ratios can only be explained by the influence of carbonatite melts (Fig. 8c, e).

Integrating the mantle source lithologies indicated by the partial melting models with oxygen isotopes leads us to conclude that the high-$\delta^{18}O$ endmember for olivine with Zr/Hf of approximately 40 corresponds to partial melts of peridotite to carbonated peridotite (Figs. 7 & 8). Thus, the EM1 component at Fogo is likely to have been tapped from a peridotite source with the influence of carbonation, supported by carbonatites also displaying high Zr/Hf, Zr/Y, Ba/Nb and high-$\delta^{18}O$ contents. In contrast, the low-$\delta^{18}O$ endmember, associated with a stronger influence from a HIMU component, shows low Zr/Hf ratios consistent with melting an eclogite source lithology (Figs. 7 & 8), which formed by recycling ocean crust into the mantle. To explain the occurrence of felsic eclogite melts we consider that experiments have shown that carbonated eclogitic sources simultaneously produce mafic and felsic partial melts. This would explain the large differences in $\delta^{18}O$ values between clinopyroxene and groundmass, and the low-$\delta^{18}O$ values of clinopyroxene compared to olivine (Dasgupta et al., 2006, 2007). Also, the carbonation of the recycled ocean crust or HIMU component is likely to have a large impact on incompatible trace elements and little influence on the $\delta^{18}O$ values, due to the abundance of oxygen in all the contributing sources compared to trace elements.

Integrating the information acquired from major and trace element geochemistry indicates that partial melting of peridotite and eclogite have contributed the main geochemical signatures. These lithologies seem to have interacted with carbonatite melts leaving their influence as carbonated peridotite and carbonated eclogite source lithologies as well as directly contributing high Ba/Th. The HIMU component, associated with eclogitic melts, is also apparent in the phonolitic glass from the

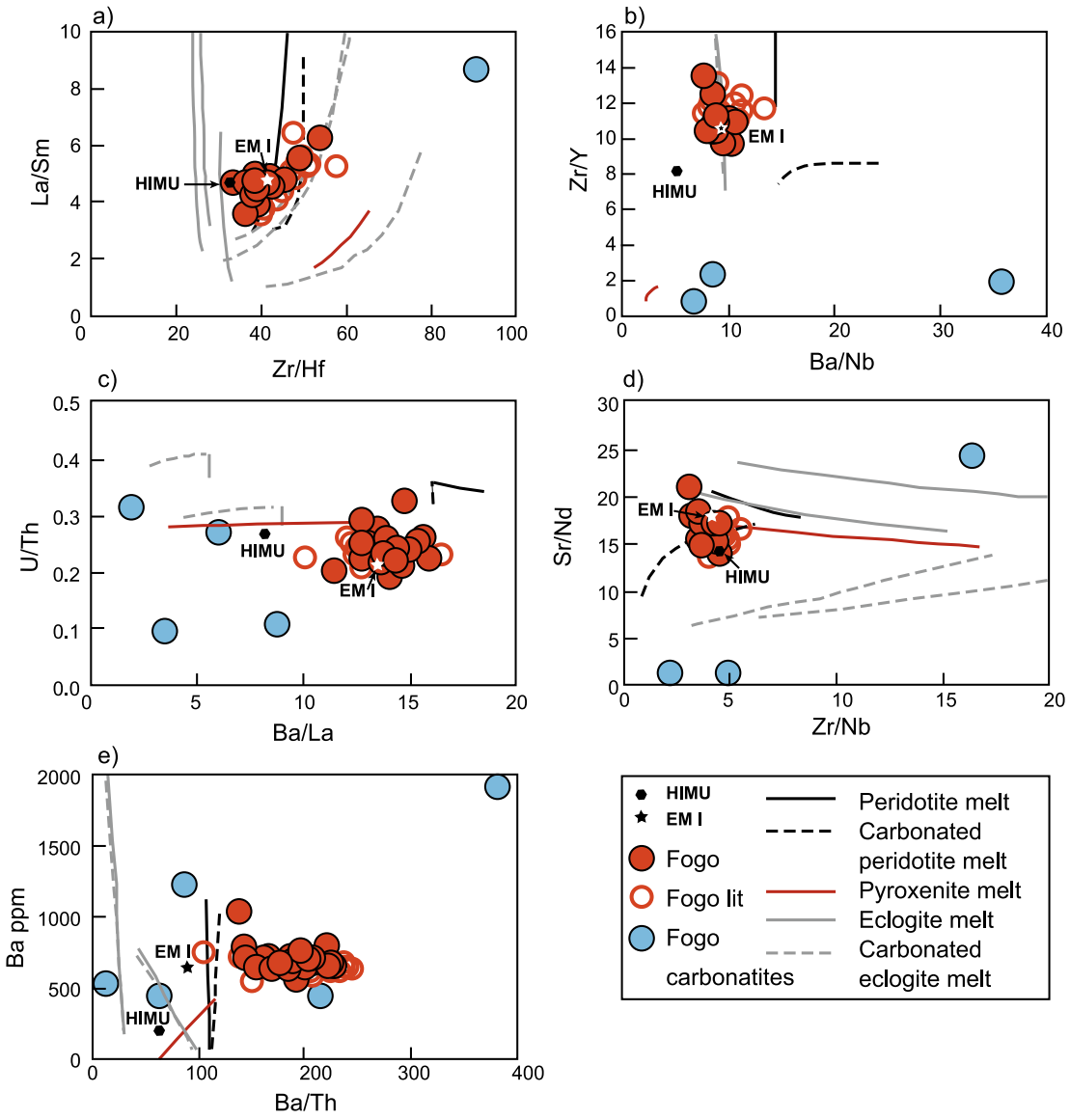


**Fig. 8.** Trace element ratios for the Fogo volcanic rocks and carbonatites compared with batch melting models for peridotite, carbonated peridotite, pyroxenite, eclogite and carbonated eclogite melts. Melting curves show 1 to 10% melting. Data sources: this study; Gerlach et al., 1988; Davies et al., 1989; Hoernle et al., 2002; Doucelance et al., 2003, 2010; Escrig et al., 2005; Hildner et al., 2011, 2012; Mata et al., 2017. See supplementary materials for information on modelling as well as partition coefficients and source compositions. (For interpretation of the references to colour in this figure legend, the reader is referred to the web version of this article.)

2014/2015 eruption and the equilibrium between clinopyroxene and felsic melt compositions. Whereas the EM1 component seems to be associated with peridotite which has been carbonated to different degrees.

## 5. Conclusions

The Fogo historic volcanic rocks show enclaves, mingling textures as well as diverse antecryst populations and oxygen isotope disequilibrium amongst antecrysts and groundmass. Distinct antecryst populations have been aggregated along with heterogeneous liquid compositions and preserve mingling of a variety of magmas. The Fogo historic volcanic rocks record HIMU, EM1 and carbonatite sources in their genesis. Recycled ocean crust contributes HIMU geochemical signatures and is associated with eclogite melts that are variably carbonated producing both felsic and mafic melts. The EM1 geochemical endmember is associated with peridotite melts that are variably carbonated, reflecting the presence of carbonatite melts which leave the hallmark of high Ba/Th.

## Declaration of Competing Interest

The authors declare that they have no known competing financial interests or personal relationships that could have appeared to influence the work reported in this paper.

## Acknowledgements

We are grateful to Herculano A. Dinis (Parque Natural do Fogo) for his help during the field work carried out in January-February 2015. We are also grateful for the assistance of Olle Risby, Uppsala University for sample preparation and Sherissa Roopnarain, UCT, for oxygen isotope analysis. We acknowledge João Mata and an anonymous reviewer for their efforts to provide highly constructive reviews. The Swedish Research Council (VR) and the Swedish Foundation for International Cooperation in Research and Higher Education (STINT) are thanked for funding the research.

## Appendix A. Supplementary data

Supplementary data to this article can be found online at https://doi.org/10.1016/j.lithos.2023.107328.

## References


Barker, A.K., Holm, P.M., Peate, D.W., Baker, J.A., 2009. Geochemical Stratigraphy of Submarine Lavas (3–5 Ma) from the Flamengos Valley, Santiago, Southern Cape Verde Islands. J. Petrol. 50, 169–193.

Barker, A.K., Holm, P.M., Peate, D.W., Baker, J.A., 2010. A 5 million year record of compositional variations in mantle sources to magmatism on Santiago, southern Cape Verde archipelago. Contrib. Mineral. Petrol. 160, 133–154.

Barker, A.K., Troll, V.R., Ellam, R.M., Hansteen, T.H., Harris, C., Stillman, C.J., Andersson, A., 2012. Magmatic evolution of the Cadamosto Seamont, Cape Verde: beyond the spatial extent of EM1. Contrib. Mineral. Petrol. 163, 949–965.

Barker, A.K., Holm, P.M., Troll, V.R., 2014. The role of eclogite in the mantle heterogeneity at Cape Verde. Contrib. Mineral. Petrol. 168 (3), 1–15.

Barker, A.K., Rydeblad, E., Silva, S.M.D.M., 2021. Magma storage at Ocean Islands: insights from Cape Verde. In: Masotta, M., Beier, C., Mollo, S. (Eds.), Crustal Magmatic System Evolution: Anatomy, Architecture and Physico-Chemical Processes AGU Monograph. https://doi.org/10.1002/9781119564485.ch3. ISBN 9781119564454.

Bindeman, I.N., Ponomareva, V.V., Bailey, J.C., Valley, J.W., 2004. Volcanic arc of Kamchatka: a province with high-δ18O magma sources and large-scale 18O/16O depletion of the upper crust. Geochim. Cosmochim. Acta 68 (4), 841–865.

Blundy, J.D., Shimizu, N., 1991. Trace element evidence for plagioclase recycling in calc-alkaline magmas. Earth Planet. Sci. Lett. 102 (2), 178–197.

Bonadiman, C., Beccaluva, L., Coltorti, M., Siena, F., 2005. Kimberlite-like metasomatism and 'garnet signature'in spinel-peridotite xenoliths from Sal, Cape Verde Archipelago: relics of a subcontinental mantle domain within the Atlantic oceanic lithosphere? J. Petrol. 46 (12), 2465–2493.

Brown, E.L., Lesher, C.E., 2016. REEBOX PRO: A forward model simulating melting of thermally and lithologically variable upwelling mantle. Geochem. Geophys. Geosyst. 17, 3929–3968. https://doi.org/10.1002/2016GC006579.

Bryce, J.G., DePaolo, D.J., 2004. Pb isotopic heterogeneity in basaltic phenocrysts. Geochim. Cosmochim. Acta 68 (21), 4453–4468.

Carracedo, J.-C., Perez-Torrado, F.J., Rodriguez-Gonzalez, A., Paris, R., Troll, V.R., Barker, A.K., 2015. Volcanic and structural evolution of Fogo, Cape Verde. Geol. Today 3, 146–152.

Carvalho, J., Silveira, G., Dumont, S., Ramalho, R., 2022. 3D-ambient noise surface wave tomography of Fogo volcano, Cape Verde. J. Volcanol. Geotherm. Res. 432, 107702.

Chiba, H., Chacko, T., Clayton, R.N., Goldsmith, J.R., 1989. Oxygen isotope fractionatioms involving diopside, forsterite, magnetite and calcite; application to goethermometry. Geochim. Cosmochim. Acta 53, 2985–2995.

Cornu, M.N., Paris, R., Doucelance, R., Bachèlery, P., Bosq, C., Auclair, D., Benbaj'kkar, M., Ganoun, A.-M., Guillou, H., 2021. Exploring the links between volcano flank collapse and the magmatic evolution of an ocean island volcano: Fogo, Cape Verde. Sci. Rep. 11 (1), 1–12.

Dalrymple, G.B., Silver, E.A., Jackson, E.D., 1973. Origin of the Hawaiian Islands: recent studies indicate that the Hawaiian volcanic chain is a result of relative motion between the Pacific plate and a melting spot in the Earth's mantle. Am. Sci. 61 (3), 294–308.

Dasgupta, R., Hirschmann, M.M., Stalker, K., 2006. Immiscible transition from carbonate-rich to silicate-rich melts in the 3 GPa melting interval of eclogite + CO2 and genesis of silica-undersaturated ocean island lavas. J. Petrol. 47, 647–671.

Dasgupta, R., Hirschmann, M.M., Smith, N.D., 2007. Partial melting experiments of peridotite+ CO2 at 3 GPa and genesis of alkalic ocean island basalts. J. Petrol. 48 (11), 2093–2124.

Davidson, J.P., Morgan, D.J., Charlier, B.L.A., Harlou, R., Hora, J.M., 2007. Microsampling and isotopic analysis of igneous rocks: implications for the study of magmatic systems. Annu. Rev. Earth Planet. Sci. 35, 273–311.

Davies, G.R., Norry, M.J., Gerlach, D.C., Cliff, R.A., 1989. A combined chemical and Pb-Sr-Nd isotope study of the Azores and Cape Verde hot-spots: the geodynamic implications. In: Saunders, A.D., Norry, M.J. (Eds.), Magmatism in Ocean Basins, 42. Geological Society of London, Special Publications, pp. 231–255.

Day, S.J., da Heleno Silva, S., Fonseca, J., 1999. A past giant lateral collapse and present-day flank instability of Fogo, Cape Verde Islands. J. Volcanol. Geotherm. Res. 94, 191–218.

DeVitre, C.L., Gazel, E., Ramalho, R.S., Venugopal, S., Steele-MacInnis, M., Hua, J., Allison, C.M., Moore, L.R., Carracedo, J.C., Monteleone, B., 2023. Oceanic intraplate explosive eruptions fed directly from the mantle. Proc. Natl. Acad. Sci. 120 (33), e2302093120.

Doucelance, R., Escrig, S., Moriera, M., Gariepy, C., Kurz, M., 2003. Pb-Sr-he isotope and trace element geochemistry of the Cape Verde Archipelago. Geochim. Cosmochim. Acta 67, 3717–3733.

Doucelance, R., Hammouda, T., Moreira, M., Martins, J.C., 2010. Geochemical constraints on depth of origin of oceanic carbonatites: the Cape Verde case. Geochim. Cosmochim. Acta 74 (24), 7261–7282.

Eiler, J.M., 2001. Oxygen isotope variations of Basaltic Lavas and upper mantle rocks. In: Valley, J.W., Cole, D.R. (Eds.), Stable Isotope Geochemistry. Reviews in Mineralogy & Geochemistry, vol. 43. Mineralogical Society of America & Geochemical Society, USA, pp. 319–364.

Eiler, J.M., Farley, K.A., Valley, J.W., Stolper, E.M., Hauri, E.H., Craig, H., 1995. Oxygen isotope evidence against bulk recycled sediment in the mantle sources of Pitcairn Island lavas. Nature 377 (6545), 138–141.

Eiler, J.M., Farley, K.A., Walley, J.F., Hauri, E., Craig, H., Hart, S.R., Stolper, E.M., 1997. Oxygen isotope variations in ocean island basalt phenocrysts. Geochem. Cosmochim. Acta. 61, 2281–2293.

Eisele, S., Freundt, A., Kutterolf, S., Hansteen, T.H., Klügel, A., Irion, I.M., 2016. Evolution of magma chambers generating the phonolitic Cão Grande Formation on Santo Antão, Cape Verde Archipelago. J. Volcanol. Geotherm. Res. 327, 436–448.

Escrig, S., Doucelance, R., Moreira, M., Allégre, C., 2005. Os isotope systematics in Fogo Island: evidence for lower continental crust fragments under the Cape Verde Southern Islands. Chem. Geol. 219, 93–113.

Fernandez, R., Faria, B., 2015. & the C4G team. FOGO-2014: monitoring the Fogo 2014 eruption, Cape Verde. Geophys. Res. Abstr. 17. EGU2015-12709.

Foeken, J., Day, S., Stuart, F., 2009. Cosmogenic $^{3}$He exposure dating of the Quaternary basalts from Fogo, Cape Verdes: implications for rift zone and magmatic reorganization. Quat. Geochronol. 4, 37–49.

Gast, P.W., 1968. Trace element fractionation and the origin of tholeiitic and alkaline magma types. Geochim. Cosmochim. Acta 32, 1057–1086.

Gerlach, D.C., Cliff, R.A., Davies, G.R., Norry, M., Hodgson, N., 1988. Magma sources of the Cape Verdes archipelago: isotopic and trace element constraints. Geochim. Cosmochim. Acta 52, 2979–2992.

González, P.J., Bagnardi, M., Hooper, A.J., Larsen, Y., Marinkovic, P., Samsonov, S.V., Wright, T.J., 2015. The 2014–2015 eruption of Fogo volcano: Geodetic modeling of Sentinel-1 TOPS interferometry. Geophys. Res. Lett. 42 (21), 9239–9246.

Guillong, M., Meier, D.L., Morray, A.M., Heinrich, C.A., Yardley, B.W.D., 2008. SILLS: a Matlab-based program for the reduction of laser ablation ICP-MS data of homogeneous materials and inclusions. Mineral. Assoc. Canada Short Course 40, 328–333.

Harris, C., Vogeli, J., 2010. Oxygen isotope composition of garnet in the Peninsula Granite, Cape Granite Suite, South Africa: constrains on melting and emplacements mechanisms. S. Afr. J. Geol. 113, 401–4012.

Harris, C., Smith, H.S., le Roex, A.P., 2000. Oxygen isotope composition of phenocrysts from Tristan da Cunha and Gough Island lavas: variation with fractional crystallization and evidence for assimilation. Contrib. Mineral. Petrol. 138 (2), 164–175.

Harris, C., le Roux, P., Cochrane, R., Martin, L., Duncan, A.R., Marsh, J.S., le Roex, A.P., Class, C., 2015. The oxygen isotope composition of Karoo and Etendeka picrites: High $\delta^{18}$O mantle or crustal contamination. Contrib. Mineral. Petrol. 170. Article 8.

Hildner, E., Klügel, A., Hauff, F., 2011. Magma storage and ascent during the 1995 eruption of Fogo, Cape Verde Archipelago. Contrib. Mineral. Petrol. 162, 751–772.

Hildner, E., Klügel, A., Hansteen, T.H., 2012. Barometry of lavas from the 1951 eruption of Fogo, Cape Verde Islands: Implications for historic and prehistoric magma plumbing systems. J. Volcanol. Geotherm. Res. 217, 73–90.

Hirose, K., Kushiro, I., 1993. Partial melting of dry peridotites at high pressure; Determination of composition of melts segregated from peridotite using aggregates of diamond. Earth Planet. Sci. Lett. 114, 447–489.

Hirschmann, M.M., Kogiso, T., Baker, M.B., Stolper, E.M., 2003. Alkalic magmas generated by partial melting of garnet pyroxenite. Geology 31, 481–484.

Hoernle, K., Tilton, G., Le Bas, M.J., Duggen, S., Garbe-Schönberg, D., 2002. Geochemistry of oceanic carbonatites compared with continental carbonatites: mantle recycling of oceanic crustal carbonate. Contrib. Mineral. Petrol. 142 (5), 520–542.

Hofmann, A.W., Jochum, K.P., Seufert, M., White, W.M., 1986. Nb and Pb in oceanic basalts: new constraints on mantle evolution. Earth Planet. Sci. Lett. 79, 33–45.

Holm, P.M., Wilson, J.R., Christensen, B.P., Hansen, L., Hansen, S.L., Hein, K.H., Mortensen, A.K., Pedersen, R., Plesner, S., Runge, M.K., 2006. Sampling the Cape Verde mantle plume: evolution of melt compositions on Santo Antão, Cape Verde Islands. J. Petrol. 47, 145–189.

Ito, E., White, W.M., Gopel, C., 1987. The O, Sr, Nd, and Pb isotope geochemistry of MORB. Chem. Geol. 62, 157–176.

Jenkins, S.F., Day, S.J., Faria, B.V.E., Fonseca, J.F.B.D., 2017. Damage from lava flows: insights from the 2014–2015 eruption of Fogo, Cape Verde. J. Appl. Volcanol. 6 (1), 6.

Klein, E.M., Langmuir, C.H., 1987. Global Correlations of Ocean Ridge Basalt Chemistry with Axial Depth and Crustal Thickness. J. Geophys. Res. 92, 8089–8115.

Klügel, A., Day, S., Schmid, M., Faria, B., 2020. Magma plumbing during the 2014–2015 eruption of Fogo (Cape Verde Islands). Frontiers. Earth Sci. 157.

Kogiso, T., Hirschmann, M.M., Reiners, P.W., 2004. Length scales of mantle heterogeneities and their relationship to ocean island basalt geochemistry. Geochim. Cosmochim. Acta 68 (2), 345–360.

Le Bas, M.J., le Maitre, R.W., Streckeisen, A., Zanettin, B., 1985. A chemical classification of volcanic rocks based on the total alkali-silica diagram. J. Petrol. 27, 745–750.

Leva, C., Rümpker, G., Link, F., Wölbern, I., 2019. Mantle earthquakes beneath Fogo volcano, Cape Verde: evidence for subcrustal fracturing induced by magmatic injection. J. Volcanol. Geotherm. Res. 386, 106672.

Martins, S., Mata, J., Munhá, J., Mendes, M.H., Maerschalk, C., Caldeira, R., Mattielli, N., 2009. Chemical and mineralogical evidence of the occurrence of mantle metasomatism by carbonate-rich melts in an oceanic environment (Santiago Island, Cape Verde). Mineral. Petrol. https://doi.org/10.1007/s00710-009-0078- x.

Mata, J., Kerrich, R., 2000. $\partial^{18}$O systematics of Madeira island basalts: petrogenetic implications. Comun. Inst. Geol. Mineiro 87, 53–62.

Mata, J., Martins, S., Mattielli, N., Madeira, J., Faria, B., Ramalho, R.S., Silva, P., Moreira, M., Caldeira, R., Rodrigues, J., Martins, L., 2017. The 2014–15 eruption and the short-term geochemical evolution of the Fogo volcano (Cape Verde): evidence for small-scale mantle heterogeneity. Lithos 288, 91–107.

Millet, M.A., Doucelance, R., Schiano, P., David, K., Bosq, C., 2008. Mantle plume heterogeneity versus shallow-level interactions: a case study, the São Nicolau Island, Cape Verde archipelago. J. Volcanol. Geotherm. Res. 176 (2), 265–276.
Mollo, S., Blundy, J., Scarlato, P., De Cristofaro, S.P., Tecchiato, V., Di Stefano, F., Vetere, F., Holtz, F., Bachmann, O., 2018. An integrated PT-H2O-lattice strain model to quantify the role of clinopyroxene fractionation on REE+ Y and HFSE patterns of mafic alkaline magmas: application to eruptions at Mt. Etna. Earth Sci. Rev. 185, 32–56.
Mourão, C., Mata, J., Doucelance, R., Maderia, J., Millet, M.A., Moreria, M., 2012. Geochemical temporal evolution of Brava Island magmatism: constraints on the variability of Cape Verde mantle sources and on carbonatite–silicate magma link. Chem. Geol. 334, 44–61.
O'Hara, M.J., 1965. Primary magmas and the origin of basalts. Scott. J. Geol. 1, 19–40.
O'Nions, R.K., Pankhurst, R.J., Grönvold, K., 1976. Nature and development of basalt magma sources beneath Iceland and the Reykjanes Ridge. J. Petrol. 17, 315–338.
Pertermann, M., Hirschmann, M.M., Hametner, K., Günther, D., Schmidt, M.W., 2004. Experimental determination of trace element partitioning between garnet and silica-rich liquid during anhydrous partial melting of MORB-like eclogite. Geochem. Geophys. Geosyst. 5 (5).
Prytulak, J., Elliott, T., 2007. $TiO_2$ enrichment in ocean island basalts. Earth Planet. Sci. Lett. 263, 388–403.
Ramalho, R., Helffrich, G., Schmidt, D.N., Vance, D., 2010. Tracers of uplift and subsidence in the Cape Verde Archipelago. J. Geol. Soc. 167 (3), 519–538.
Richter, N., Favalli, M., de Zeeuw-van Dalfsen, E., Fornaciai, A., da Silva Fernandes, R. M., Levy, J., Walter, T.R., 2016. Lava flow hazard at Fogo Volcano, Cabo Verde, before and after the 2014–2015 eruption. Nat. Hazards Earth Syst. Sci. 16 (8), 1925–1951.
Ryan, W.B., Carbotte, S.M., Coplan, J.O., O'Hara, S., Melkonian, A., Arko, R., Weissel, R. A., Ferrini, V., Goodwillie, A., Nitsche, F., Bonczkowski, J., 2009. Global multi-resolution topography synthesis. Geochem. Geophys. Geosyst. 10 (3).
Sobolev, A.V., Hofmann, A.W., Nikogosian, I.K., 2000. Recycled oceanic crust observed in 'ghost plagioclase' within the source of Mauna Loa lavas. Nature 404 (6781), 986–990.
Sobolev, A.V., Hofmann, A.W., Sobolev, S.V., Nikogosian, I.K., 2005. An olivine-free mantle source of Hawaiian shield basalts. Nature 434 (7033), 590–597.
Spandler, C., Yaxley, G., Green, D.H., Rosenthal, A., 2008. Phase relations and melting of anhydrous K-bearing eclogite from 1200 to 16008C and 3 to 5 GPa. J. Petrol. 49 https://doi.org/10.1093/petrology/egm039, 771ˆ795.
Taylor Jr., H.P., Frechen, J., Degens, E.T., 1967. Oxygen and carbon isotope studies of carbonatites from the Laacher See District, West Germany and the Alnö District, Sweden. Geochim. Cosmochim. Acta 31 (3), 407–430.
Taylor, R.P., Jackson, S.E., Longerich, J.P., Webster, J.D., 1997. In situ trace-element analysis of individual silicate melt inclusions by laser ablation microprobe-inductively coupled plasma-mass spectrometry (LAM-ICP-MS). Geochim. Cosmochim. Acta 61, 2559–2567.
Tepley III, F.J., Davidson, J.P., Clynne, M.A., 1999. Magmatic interactions as recorded in plagioclase phenocrysts of Chaos Crags, Lassen Volcanic Center, California. J. Petrol. 40 (5), 787–806.
Woodhead, J.D., Greenwood, P., Harmon, R.S., Stoffers, P., 1993. Oxygen isotope evidence for recycled crust in the source of EM-type Ocean island basalts. Nature 362 (6423), 809–813.
Worsley, P., 2015. Physical geology of the Fogo volcano (Cape Verde Islands) and its 2014-2015 eruption. Geol. Today 31, 153–159.
Zhao, Z.F., Zheng, Y.F., 2003. Calculation of oxygen isotope fractionation in magmatic rocks. Chem. Geol. 193 (1–2), 59–80.